

# Camera Pose Estimation and Reconstruction from Image Profiles under Circular Motion

Paulo R. S. Mendonça, Kwan-Yee K. Wong, and Roberto Cipolla

Department of Engineering, University of Cambridge  
Trumpington Street, Cambridge, UK, CB2 1PZ  
{prdsm2, kykw2, cipolla}@eng.cam.ac.uk

**Abstract.** This paper addresses the problem of motion estimation and reconstruction of 3D models from profiles of an object rotating on a turntable, obtained from a single camera. Its main contribution is the development of a practical and accurate technique for solving this problem from profiles alone, which is, for the first time, precise enough to allow the reconstruction of the object. No correspondence between points or lines are necessary, although the method proposed can be equally used when these features are available, without any further adaptation. Symmetry properties of the surface of revolution swept out by the rotating object are exploited to obtain the image of the rotation axis and the homography relating epipolar lines, in a robust and elegant way. These, together with geometric constraints for images of rotating objects, are then used to obtain first the image of the horizon, which is the projection of the plane that contains the camera centres, and then the epipoles, thus fully determining the epipolar geometry of the sequence of images. The estimation of the epipolar geometry by this sequential approach (image of rotation axis — homography — image of the horizon — epipoles) avoids many of the problems usually found in other algorithms for motion recovery from profiles. In particular, the search for the epipoles, by far the most critical step, is carried out as a simple one-dimensional optimisation problem. The initialisation of the parameters is trivial and completely automatic for all stages of the algorithm. After the estimation of the epipolar geometry, the Euclidean motion is recovered using the fixed intrinsic parameters of the camera, obtained either from a calibration grid or from self-calibration techniques. Finally, the spinning object is reconstructed from its profiles, using the motion estimated in the previous stage. Results from real data are presented, demonstrating the efficiency and usefulness of the proposed methods.

## 1 Introduction

Methods for motion estimation and 3D reconstruction from point or line correspondences in a sequence of images have achieved a high level of sophistication, with impressive results [12, 8]. Nevertheless, if corresponding points are not available the current techniques cannot be applied. That is exactly the case when the scene being viewed is composed by non-textured smooth surfaces, and in this situation the predominant feature in the image is the *profile* or *apparent contour* of the surface [13]. Besides, even when point correspondences can be established, the profile still offers important clues for determining both motion and shape, and therefore should be used whenever available.

This work presents a method for motion estimation and reconstruction of an object rotating around a fixed axis from information provided by its profiles. It makes use of symmetry properties of the surface of revolution swept out by the rotating object to overcome the main difficulties and drawbacks present in other methods which have attempted to estimate motion from apparent contours, namely: the need for a very good initialisation for the epipolar geometry and an unrealistic demand of a large number of *epipolar tangencies* [5, 1, 2] (here as few as two epipolar tangencies are needed), restriction to linear motion [18] (whereas circular motion is a more practical situation), or the use of an affine approximation

[14, 22] (which may be used only for shallow scenes). After obtaining the motion, the reconstruction can be achieved by a simple technique, based on the epipolar parameterisation [6], which extends the common triangulation methods from points to profiles.

The first attempts to approach the problem of motion estimation from apparent contours date back to Rieger, in 1986 [17], who introduced the concept of *frontier point*, interpreted as “centres of spin” [*sic*] of the image motion. The paper dealt with the case of fronto-parallel orthographic projection, which is a rather restrictive situation. This idea was further developed by Porrill [16], who recognised the frontier point as a fixed point on the surface, corresponding to the intersection of two consecutive *contour generators* [6]. The connection between the epipolar geometry and the frontier points was established in [10], and an algorithm for motion estimation from profiles was introduced in [5].

Related works also include [1], where a technique based on registering the images using a planar curve was first developed. This method was implemented in [7], which also showed results of reconstruction from the estimated motion. In [14] the algorithm presented in [5] is specialised to the affine case.

The first steps towards a solution for the problem of reconstruction from apparent contours with known camera motion were given by Barrow and Tenenbaum, in 1981 [3], where a technique to compute surface normals was introduced. Koenderink [13] established relations between the differential geometry of a surface and the differential geometry of its profiles. This work was extended in [9], where algorithms for computing the curvature of a surface from its profiles were developed and implemented for orthographic projection.

In [20] a reconstruction method based on parameterising the surface by *radial curves* was developed. Better results can be achieved by using an *epipolar parameterisation*, together with an interpolation using the *osculating circle*, as introduced in [6]. Further refinements were obtained in [4], and a simple technique was developed in [22], based on a finite-difference implementation of [6]. Despite its simplicity, the method developed in [22] renders results comparable to those in [4] and [6], and was thus the technique chosen to be used here.

An interesting comparison can be made between the work presented here and [8]. Both papers tackle the same problem, but while in [8] hundreds of points are tracked and matched for each pair of adjacent images, it is shown here that a solution can be obtained even when only two epipolar tangencies are available, with at least comparable results.

Section 2 presents a summary of the theoretical background and notation used in the remaining of the paper. It reviews the symmetry properties of images of surfaces of revolution related to the *harmonic homology*, and presents two useful parameterisations of the fundamental matrix. These parameterisations allow the estimation of the epipoles to be carried out as independent one-dimensional searches, avoiding points of local minima. This greatly reduces the computational complexity of the estimation. Section 3 presents the algorithm for motion recovery, and the implementation of the algorithm for real data is shown in Section 4, which also makes comparisons with previous works. The reconstruction technique is described in Section 5, together with experimental results for reconstruction.

## 2 Theoretical Background

This section is a concise review of the mathematical background necessary for the rest of the paper, and only the main results will be presented. Details of the derivations can be found in [15].

### 2.1 Symmetry Properties of Images of Surfaces of Revolution

A 2D homography that keeps the pencil of lines through a point  $\mathbf{u}$  and the set of points on a line  $\mathbf{l}$  fixed is called a *perspective collineation* with centre  $\mathbf{u}$  and axis  $\mathbf{l}$ . A *homology* is a perspective collineation whose centre and axis are not incident (otherwise the perspective

homology is called *elation*). Let  $\mathbf{x}$  be a point mapped by an homology onto a point  $\mathbf{x}'$  and let  $\mathbf{q}$  be the line passing through these points. The point of intersection of  $\mathbf{q}$  and  $\mathbf{l}$  is denoted by  $\mathbf{v}$ . If  $\mathbf{x}$  and  $\mathbf{x}'$  are harmonic conjugates with respect to  $\mathbf{u}$  and  $\mathbf{v}$ , i.e., their cross-ratio is one, the homology is said to be a *harmonic homology* (see details in [19, Chapter IX]). A curve or set of points invariant to a harmonic homology will be henceforth called *harmonically symmetric*.

Consider an object rotating about a fixed axis. The surface of the object sweeps out a surface of revolution  $S$ . The image of  $S$  taken by a pinhole camera  $\mathbf{P}$  is a curve  $s$ . Let  $\mathbf{l}_s$  be the image of the axis of rotation of the surface  $S$  in the camera  $\mathbf{P}$ . The optical centre of  $\mathbf{P}$  and the axis of rotation define a plane  $\Psi$ , whose normal direction is  $\mathbf{n}_\Psi$ . The image of the point at infinity in the direction  $\mathbf{n}_\Psi$  is the vanishing point  $\mathbf{v}_x$ .

If  $\mathbf{v}_x$  and  $\mathbf{l}_s$  are represented in homogeneous coordinates, the 2D collineation  $\mathbf{W}$  given by

$$\mathbf{W} = \mathbb{I} - 2 \frac{\mathbf{v}_x \mathbf{l}_s^T}{\mathbf{v}_x^T \mathbf{l}_s} \quad (1)$$

is a harmonic homology, and  $s$  is harmonically symmetric with respect to  $\mathbf{W}$ . It is worth remembering that  $\mathbf{W}$  is an involutory matrix, i.e.,  $\mathbf{W}^2 = \mathbb{I}$ . It can be shown that if the camera  $\mathbf{P}$  points towards the axis of rotation, the harmonic homology  $\mathbf{W}$  reduces to a skew symmetry transformation, and the curve  $s$  will simply be skew symmetric about  $\mathbf{l}_s$ . Furthermore, if the camera aspect ratio is one and the skew is zero, the skew symmetry transformation becomes a mirroring, and the curve  $s$  will be bilaterally symmetrical about  $\mathbf{l}_s$ , as shown in Figure 1.

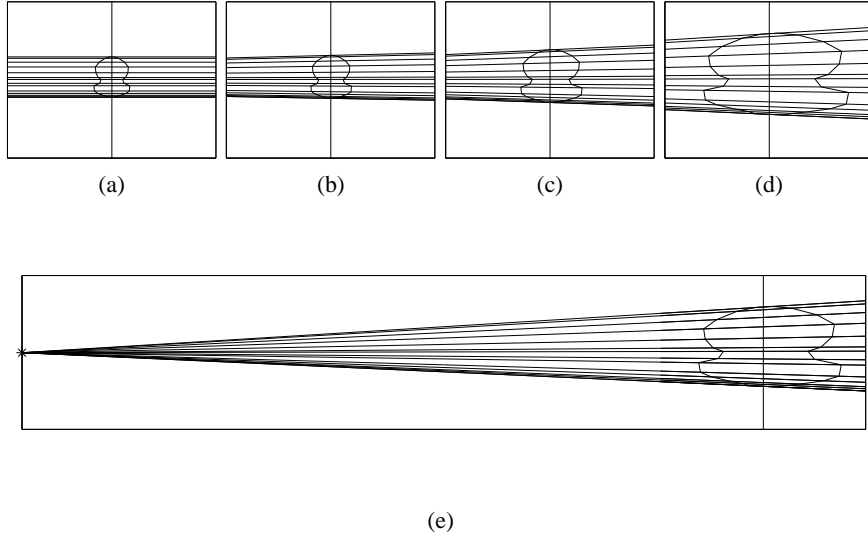


**Fig. 1.** Lines joining points which are symmetric about the image of rotation axis  $\mathbf{l}_s$  (images are scaled and translated independently for better observation). (a) The optical axis points directly towards the rotation axis. (b) The camera is rotated about its optical centre by an angle  $\rho$  of  $20^\circ$  in a plane orthogonal to the rotation axis. (c)  $\rho = 40^\circ$ . (d)  $\rho = 60^\circ$ . (e) Same as (d), but the vanishing point  $\mathbf{v}_x$  is also shown.

## 2.2 Parameterisations of the Fundamental Matrix

Consider a pair of camera matrices  $\mathbf{P}_1$  and  $\mathbf{P}_2$  related by a rotation with an angle  $\theta \neq 0$  about an axis  $\mathbf{a}$  not passing through their optical centres, represented as the matrix  $\mathbf{R}_a^\theta$ .

The image of the plane containing the optical centres of the cameras and orthogonal to the axis  $a$  is the *horizon*, and it is represented as the line  $\mathbf{l}_h$  in homogeneous coordinates. The fundamental matrix  $\mathbf{F}$  relating  $\mathbf{P}_1$  and  $\mathbf{P}_2$  is given by (see [21, 8])

$$\mathbf{F} = [\mathbf{v}_x]_{\times} + k \tan \frac{\theta}{2} (\mathbf{l}_s \mathbf{l}_h^T + \mathbf{l}_h \mathbf{l}_s^T), \quad (2)$$

with  $\mathbf{l}_h^T \mathbf{v}_x = 0$ , using the notation of Section 2.1. The parameter  $k$  is unknown but fixed for any angle  $\theta$ , and cannot be obtained from two images alone. This should be expected, since the terms in (2) are in homogeneous coordinates, and thus defined only up to arbitrary scale factors.

From (2) it is easy to prove that the epipole  $\mathbf{e}_i$ , formed in the image of camera  $\mathbf{P}_i$ , is given by

$$\mathbf{e}_i = \mathbf{v}_x - (-1)^i k \tan \frac{\theta}{2} [\mathbf{l}_s]_{\times} \mathbf{l}_h. \quad (3)$$

From (3) it can be seen that all the epipoles lie on the horizon  $\mathbf{l}_h$ , independently of the value of  $\theta$ . It can also be shown that the parameterisation given by (2) is equivalent to

$$\mathbf{F} = [\mathbf{e}_2]_{\times} \mathbf{W}, \quad (4)$$

where  $\mathbf{W}$  is given by (1), and, moreover,  $\mathbf{e}_1 = \mathbf{W}\mathbf{e}_2$ . The result in (4) shows that there is a plane in space that induces the homology  $\mathbf{W}$ . The proof of the following theorem does not appear anywhere else, and it will be shown here in more detail.

**Theorem 1.** *The planar homology  $\mathbf{W}$  relating the cameras  $\mathbf{P}_1$  and  $\mathbf{P}_2$  with  $\theta \neq n\pi$ ,  $n \in \mathbb{Z}$ , is induced by the plane  $\mathcal{E}$  that contains the axis of rotation  $\mathbf{a}$  and bisects the segment joining the optical centres of the cameras.*

*Proof.* The existence and uniqueness of  $\mathcal{E}$  satisfying the hypothesis of the Theorem are trivial. Let  $\mathbf{x}_1 = [1 \ 0 \ 0]^T$ ,  $\mathbf{x}_2 = [0 \ 1 \ 0]^T$ , and  $\mathbf{x}_3 = [0 \ 0 \ 1]^T$ . Without loss of generality, let

$$\begin{aligned} \mathbf{P}_1 &= \mathbf{K}\mathbf{R}[\mathbb{I} \mid \mathbf{x}_3] \quad \text{and} \\ \mathbf{P}_2 &= \mathbf{K}\mathbf{R}[\mathbf{R}_y^\theta \mid \mathbf{x}_3], \end{aligned} \quad (5)$$

where  $\mathbf{K}$  is the intrinsic parameters matrix of  $\mathbf{P}_1$  and  $\mathbf{P}_2$ ,  $\mathbf{R}$  is the rotation matrix relating the orientation of the coordinate system of  $\mathbf{P}_1$  to the world coordinate system, and  $\mathbf{R}_y^\theta$  is a rotation by  $\theta$  about the  $y$ -axis of the world coordinate system, i.e.,

$$\mathbf{R}_y^\theta = \begin{bmatrix} \cos \theta & 0 & \sin \theta \\ 0 & 1 & 0 \\ -\sin \theta & 0 & \cos \theta \end{bmatrix}. \quad (6)$$

Therefore,  $\forall \alpha, \beta \in \mathbb{R}$ , the point  $\mathbf{X} = [-\alpha \sin(\theta/2) \ \beta \ \alpha \cos(\theta/2)]^T$  lies on  $\mathcal{E}$ . Projecting  $\mathbf{X}$  using  $\mathbf{P}_1$  and  $\mathbf{P}_2$ , one obtains  $\mathbf{u}_1 = \mathbf{K}\mathbf{R}(\mathbf{X} + \mathbf{x}_3)$  and  $\mathbf{u}_2 = \mathbf{K}\mathbf{R}(\mathbf{R}_y^\theta \mathbf{X} + \mathbf{x}_3)$ . Since

$$\begin{aligned} \mathbf{R}_y^\theta \mathbf{X} &= \begin{bmatrix} \alpha \sin \theta \cos(\theta/2) - \alpha \cos \theta \sin(\theta/2) \\ \beta \\ \alpha \sin \theta \sin(\theta/2) + \alpha \cos \theta \cos(\theta/2) \end{bmatrix} \\ &= \begin{bmatrix} \alpha \sin(\theta/2) \\ \beta \\ \alpha \cos(\theta/2) \end{bmatrix} = \begin{bmatrix} -1 & 0 & 0 \\ 0 & 1 & 0 \\ 0 & 0 & 1 \end{bmatrix} \mathbf{X}, \end{aligned} \quad (7)$$

or  $\mathbf{R}_y^\theta \mathbf{X} = (\mathbb{I} - 2\mathbf{x}_1 \mathbf{x}_1^T) \mathbf{X}$ , we have  $\mathbf{u}_2 = \mathbf{K}\mathbf{R}[(\mathbb{I} - 2\mathbf{x}_1 \mathbf{x}_1^T) \mathbf{X} + \mathbf{x}_3]$ , or  $\mathbf{u}_2 = (\mathbb{I} - 2\mathbf{K}\mathbf{R}\mathbf{x}_1 \mathbf{x}_1^T \mathbf{R}^{-1} \mathbf{K}^{-1}) \mathbf{u}_1$ . It can be shown [15] that  $\mathbf{K}\mathbf{R}\mathbf{x}_1 = \mathbf{v}_x$  and  $\mathbf{x}_1^T \mathbf{R}^{-1} \mathbf{K}^{-1} = \mathbf{l}_s^T$ , and thus the result follows.  $\square$

### 2.3 Epipolar Geometry and Apparent Contours

Consider a surface  $\mathcal{S}$  of type  $C^1$  viewed by two pinhole cameras  $\mathbf{P}_1$  and  $\mathbf{P}_2$ . The following definitions are presented as a quick review:

- a *contour generator* associated with the surface  $\mathcal{S}$  and the camera  $\mathbf{P}_1$  corresponds to the space curve  $\mathcal{C} \subset \mathcal{S}$  such that for all points  $c \in \mathcal{C}$  the line passing through the optical centre of  $\mathbf{P}_1$  and  $c$  is tangent to  $\mathcal{S}$  at  $c$ ;
- the image of the contour generator associated with a camera  $\mathbf{P}_1$  on this same camera is a *profile* or *apparent contour*;
- if two contour generators associated with the surface  $\mathcal{S}$  and the cameras  $\mathbf{P}_1$  and  $\mathbf{P}_2$  intersect, the points of intersection are denoted *frontier points*;
- the epipolar plane  $\Pi$  defined by the optical centres of the two cameras  $\mathbf{P}_1$  and  $\mathbf{P}_2$  and the frontier point is tangent to the associated surface  $\mathcal{S}$ ;
- the epipolar lines corresponding to the epipolar plane  $\Pi$  are tangent to their associated apparent contours and are called *epipolar tangents*;

The tangent point of associated epipolar tangencies corresponds to the image of the same point on the surface  $\mathcal{S}$ , namely the frontier point. All the above definitions can be better understood by looking at Figure 2.

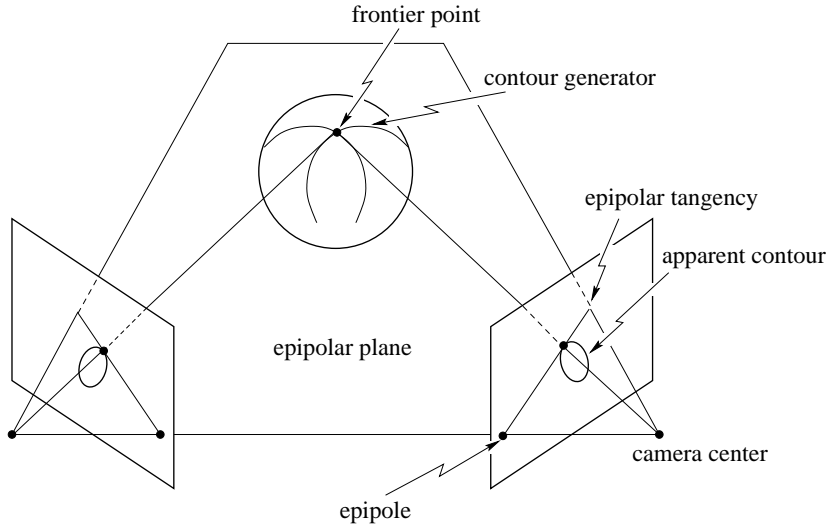


**Fig. 2.** The frontier point is a fixed point on the surface, corresponding to the intersection of two contour generators. The epipolar lines corresponding to the frontier point are tangent to the profile.

### 3 Motion Estimation

Consider an object that undergoes a full rotation around a fixed axis. The envelope  $\epsilon$  of its profiles is found by overlapping the images of the sequence and applying a Canny edge detector to the resultant image (Figure 3(b)). This envelope corresponds to the image of a surface of revolution, and thus it is harmonically symmetric. The homography  $\mathbf{W}$  related to  $\epsilon$  is then found by sampling  $N$  points  $\mathbf{x}_i$  along  $\epsilon$  and optimising the cost function

$$f_{\mathbf{W}}(\mathbf{v}_x, \mathbf{l}_s) = \sum_{i=1}^N \text{dist}(\epsilon, \mathbf{W}(\mathbf{v}_x, \mathbf{l}_s)\mathbf{x}_i)^2, \quad (8)$$

where  $\text{dist}(\epsilon, \mathbf{W}(\mathbf{v}_x, \mathbf{l}_s)\mathbf{x}_i)$  is the distance between the curve  $\epsilon$  and the transformed sample point  $\mathbf{W}(\mathbf{v}_x, \mathbf{l}_s)\mathbf{x}_i$ .

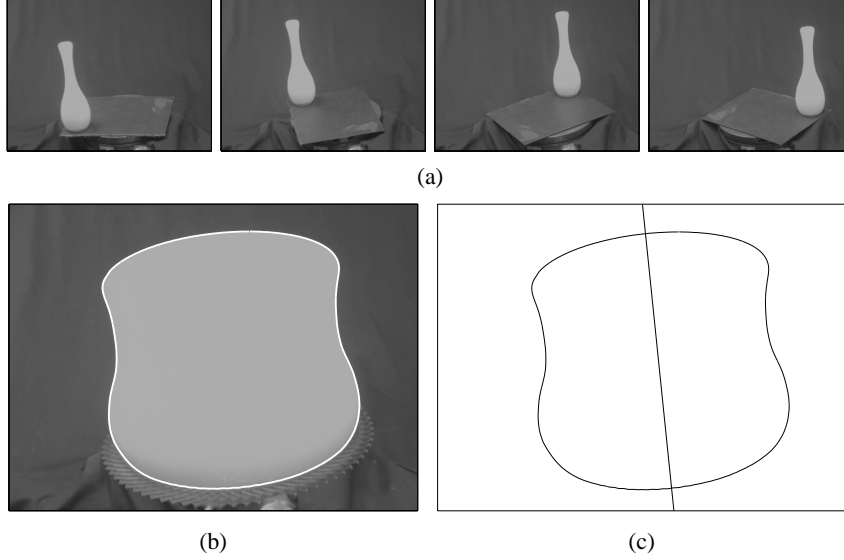


**Fig. 3.** (a) Image 1, 8, 15 and 22 in the sequence of 36 images of a rotating vase. (b) Envelope of apparent contours produced by overlapping all images in the sequence. (c) Estimation of the image of the rotation axis.

The initialisation of the line  $\mathbf{l}_s$  and the point  $\mathbf{v}_x$  can be made very close to the global minimum by automatically locating one or more pairs of corresponding bitangents on the envelope. The estimation of  $\mathbf{W}$  is summarised in Algorithm 1.

---

**Algorithm 1** Estimation of the harmonic homology  $\mathbf{W}$ .

---

```

overlap the images in sequence;
extract the envelope  $\epsilon$  of the profiles using a Canny edge detector;
sample  $N$  points  $\mathbf{x}_i$  along  $\epsilon$ ;
initialise the axis of symmetry  $\mathbf{l}_s$  and the vanishing point  $\mathbf{v}_x$  using bitangents
while not converged do
  transform the points  $\mathbf{x}_i$  using  $\mathbf{W}$ ;
  compute the distances between  $\epsilon$  and the transformed points;
  update  $\mathbf{l}_s$  and  $\mathbf{v}_x$  to minimise the function in (8);
end while

```

---

After obtaining a good estimation of  $\mathbf{W}$ , one can then search for *epipolar tangencies* between pairs of images in the sequence using the parameterisation given by (4). To obtain a pair of corresponding epipolar tangents in two images, it is necessary to find a line tangent to one profile which is transformed by  $\mathbf{W}^{-T}$  onto a line tangent to the profile in the other image (see Figure 4). The search for corresponding tangents may be carried out as a one-dimensional optimisation problem. The single parameter is the angle  $\alpha$  that defines the orientation of the epipolar line  $\mathbf{l}$  in the first image, and the cost function is given by

$$f_\alpha = \text{dist}(\mathbf{W}^{-T}\mathbf{l}(\alpha), \mathbf{l}'_\parallel(\alpha)), \quad (9)$$

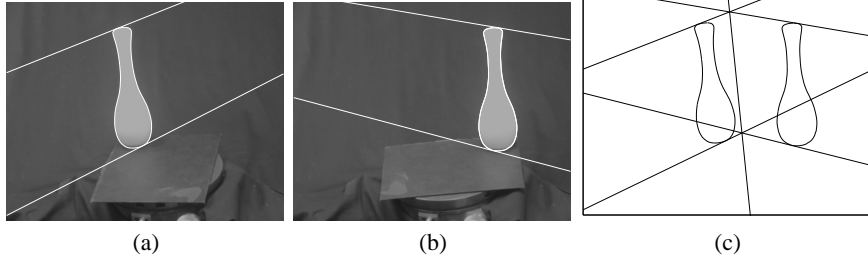


**Fig. 4.** A pair of images of an object undergoing circular motion with a rotation of  $80^\circ$  is shown in (a) and (b). The overlapping of the two images can be seen in (c). Corresponding epipolar lines intersect at the image of the rotation axis, and all epipoles lie on a common horizon.

where  $\text{dist}(\mathbf{W}^{-T}\mathbf{l}(\alpha), \mathbf{l}'_{\parallel}(\alpha))$  is the distance between the transformed line  $\mathbf{l}' = \mathbf{W}^{-T}\mathbf{l}$  and a parallel line  $\mathbf{l}'_{\parallel}$  tangent to the profile in the second image. Typical values of  $\alpha$  lie between  $-0.5$  rad and  $0.5$  rad, or  $-30^\circ$  and  $30^\circ$ . The shape of the cost function (9) for the profiles in Figure 4 can be seen in Figure 5.

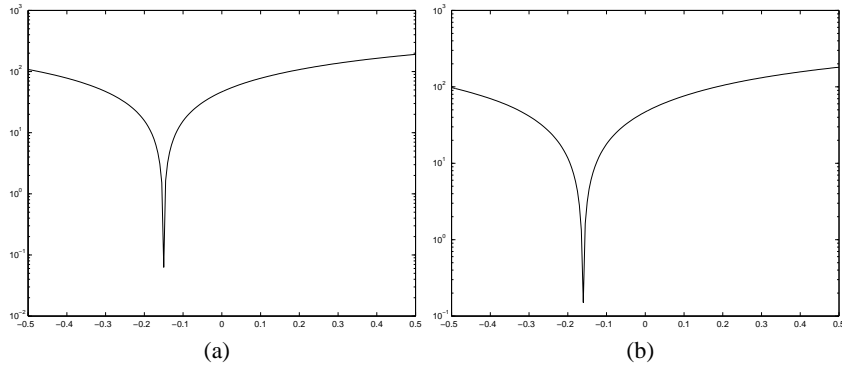


**Fig. 5.** Plot of the cost function (9) for a pair of images in the sequence. (a)/(b) Cost function for a pair of corresponding epipolar tangents near the top/bottom of the profile in Figure 4.

---

**Algorithm 2** Estimation of the orientation of the epipolar lines.

---

```

extract the profiles of two adjacent images using a Canny edge detector;
fit b-splines to the top and the bottom of the profiles;
initialise  $\alpha$ ;
while not converged do
  find  $\mathbf{l}$ ,  $\mathbf{l}'$  and  $\mathbf{l}'_{\parallel}$ ;
  compute the distance between  $\mathbf{l}'$  and  $\mathbf{l}'_{\parallel}$ ;
  update  $\alpha$  to minimise the function in (9);
end while

```

---

The epipoles can then be computed as the intersection of epipolar lines at the same image. After obtaining this first estimate for the epipoles, the image of the horizon can then be found by robustly fitting a line  $\mathbf{l}_h$  to the initial set of epipoles, such that  $\mathbf{l}_h^T \mathbf{v}_x$ .

An alternative method to compute the epipoles is to register the profiles using the homology  $\mathbf{W}$ , eliminating the effects of rotation on the images, and then apply any of the methods in [1, 18, 7], in a *plane + parallax* approach. However, no advantage has been obtained by doing so, since to use this method it is necessary to search for a common tangent between two profiles, which involves a search at least as complex as the one in Algorithm 2.

Figure 7 shows a typical output of Algorithm 2, together with the horizon  $\mathbf{l}_h$  fitted to the epipoles. After estimating the horizon, the only missing term in the parameterisation of the fundamental matrix shown in (2) is the scale factor  $k \tan \theta/2$ . This parameter can be found by, again, a one-dimensional search that minimises the geometric error of transformed epipolar lines as shown in Fig 6.

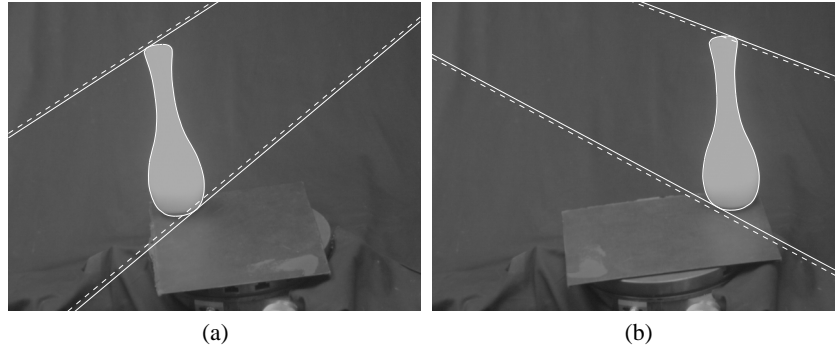


**Fig. 6.** Geometric error for transformed epipolar lines, with the scale factor  $k \tan \theta/2$  in (3) set to 100, for better visualisation. The terms  $\mathbf{v}_x$ ,  $\mathbf{l}_s$  and  $\mathbf{l}_h$  were obtained from Algorithm 1 and Algorithm 2. The solid lines in each correspond to tangents to the profile passing through the epipoles, and the dashed lines correspond to lines transferred from the one image to the other by applying the harmonic homology  $\mathbf{W}$ . The distance between transformed lines and the corresponding tangent points is the cost function that drives the search for the scale factor  $k \tan \theta/2$  in (3).

## 4 Implementation and Experimental Results

The algorithms described in the previous session were tested using a set of 36 images of a vase placed on a turntable (see Figure 3(a)) rotated by an angle of  $10^\circ$  between successive snapshots. To obtain  $\mathbf{W}$ , Algorithm 1 was implemented with 100 evenly spaced sample points along the envelope ( $N = 100$ ). Bitangents were used to find an initial guess for homology  $\mathbf{W}$ . Less than 10 iterations of the Levenberg-Marquadt algorithm are necessary, with derivatives computed by finite differences. The final configuration of the rotation axis can be seen in Figure 3(c).

In the implementation of Algorithm 2, 70 pairs of images were selected by uniformly sampling the indexes of the images, and the resultant estimate for the epipoles is shown in Figure 7, which also shows the horizon  $\mathbf{l}_h$  found by a robust fit. To get  $\mathbf{l}_h$  a minimisation of the median of the squares of the residuals was used, followed by removal of outliers and orthogonal least-squares regression using the remaining points (inliers). The epipolar geometry was then re-estimated with the epipoles constrained to lie on  $\mathbf{l}_h$ . The resulting camera configurations are presented in Figure 8.

The object was rotated on a manual turntable with resolution of  $0.01^\circ$ , but the real precision achieved is highly dependent on the skills of the operator. The RMS error in the estimated angles is less than  $0.2^\circ$ , as can be seen from Figure 9, demonstrating the accuracy of the estimation.

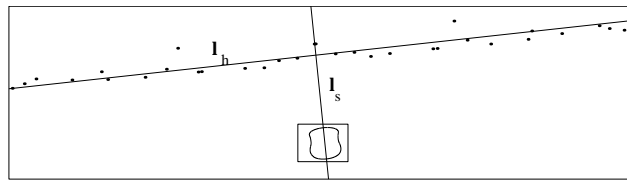


**Fig. 7.** Epipoles estimated by Algorithm 2. The horizon is found by doing a robust fit to the cloud of epipoles.

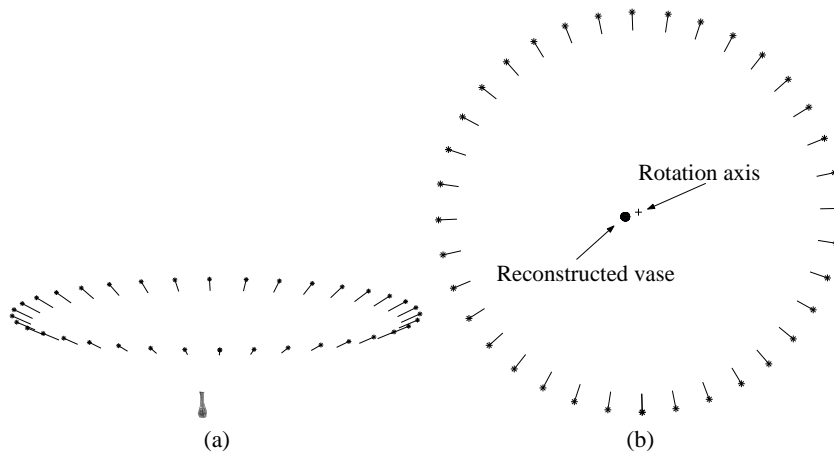


**Fig. 8.** Lateral and top view of the estimated configuration of the cameras. The technique to reconstruct the object shown at the bottom in (a) and in the centre in (b) is described in Section 5.

It is interesting to compare this result with the ones shown in [8, pg. 166] for the “Head”, “Freiburg” and “Dinosaur” sequences, where the average number of point matches per image pair varies from 137 to 399, depending on the sequence. It should be stressed that only two epipolar tangents were used for each pair of images in the experiments presented in this paper, with comparable results.

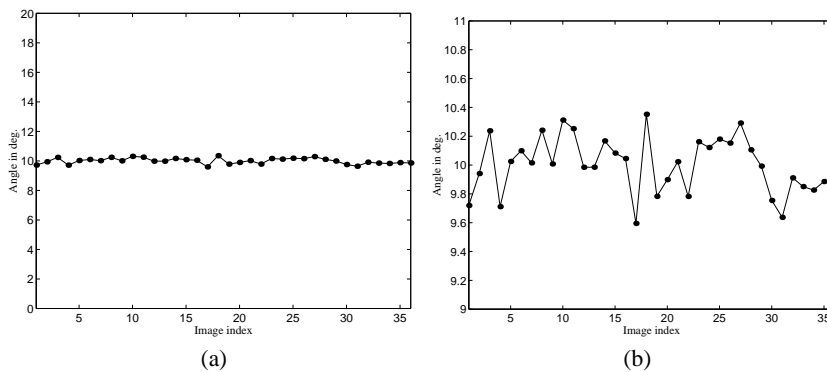


**Fig. 9.** Estimated angle of rotation between successive views. The RMS error is  $0.2^\circ$ , for a maximum resolution of  $0.01^\circ$  for the manual turntable.

## 5 Reconstruction from Image Profiles

The algorithm for motion estimation introduced here can perfectly be used even when point correspondences can be established. On the other hand, methods as the ones in [8] and [12] cannot deal with situations where profiles are the only available features in the scene, and it is therefore natural to use the motion recovered by the technique shown in this paper to the problem of reconstruction from apparent contours. To solve this problem under known motion, the main algorithms can be found in [20, 6, 4, 22]. Results reported in [22] compare the last three, and although it slightly favours the one in [4], the simplicity of the method proposed in [22] justifies its choice for evaluating the accuracy of the motion estimated here.

### 5.1 Description of the Method

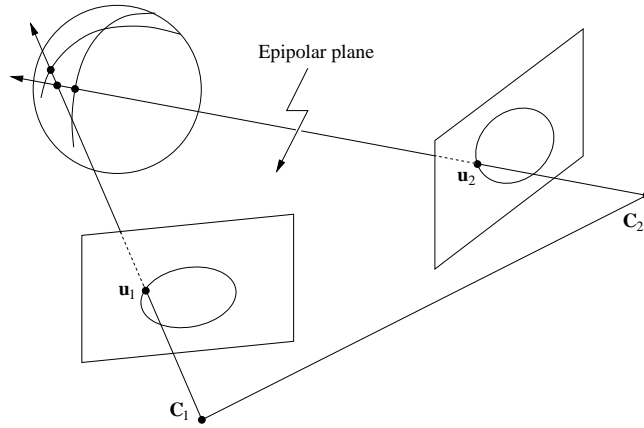


**Fig. 10.** The correspondence between the points  $\mathbf{u}_1$  and  $\mathbf{u}_2$  is established via the epipolar parameterisation. The result of the triangulation of  $\mathbf{u}_1$  and  $\mathbf{u}_2$  is *not* a point on the surface, but if the motion is small, the error will be negligible.

The algorithm for reconstruction from apparent contours introduced in [22] is based on the assumption that, if the motion is small, the error in triangulating correspondences on images of successive contour generators, established via the epipolar parameterisation, will be negligible (see Figure 10). This corresponds to a finite-difference approximation of the technique shown in [6]. A summary of the procedure is shown in Algorithm 3.

---

#### Algorithm 3 Reconstruction from image profiles.

---

```

for  $i = 1$  to  $N - 1$  do
  sample  $M$  points  $\mathbf{u}_j$  along the profile of image  $i$ ;
  for  $j = 1$  to  $M$  do
    compute the epipolar line  $\mathbf{l}$  at image  $i + 1$  corresponding to the point  $\mathbf{u}_j$ ;
    find the intersection  $\mathbf{u}'_j$  of the line  $\mathbf{l}$  with the profile in image  $i + 1$ ;
    triangulate the points  $\mathbf{u}_j$  and  $\mathbf{u}'_j$ ;
  end for
end for

```

---

## 5.2 Implementation and Experimental Results

A B-spline was fitted to the left side of the profile in the sequence of images shown in Figure 3(a). From the top to the bottom, 18 points were sampled on the spline in the first image (see Figure 11(a)), from which the corresponding epipolar lines in the second image were computed, and associated points were then triangulated. The intersection of the epipolar lines with the profile at the second image is shown in Figure 11(b). Since the points satisfy the epipolar constraint by construction, the triangulation will be exact, i.e., the rays associated with the points at the first image will exactly intersect the corresponding rays at the second image. As pointed in [11], in this case the choice of triangulation method becomes irrelevant, and a simple least-squares solution was adopted.

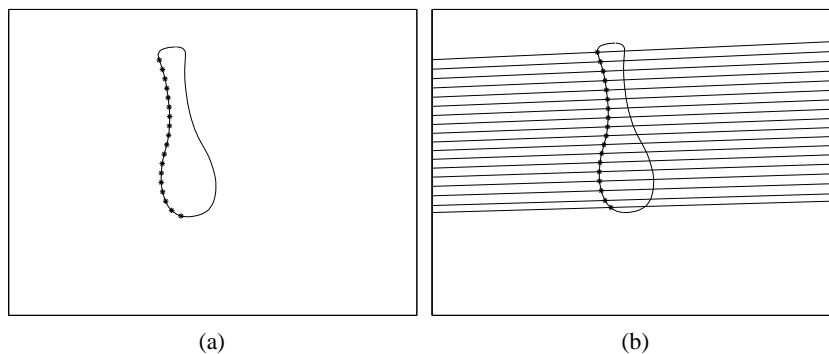


**Fig. 11.** (a) Points sampled at the first image. (b) Corresponding epipolar lines at the second image. The triangulation is carried out between a point in the first image and the intersection of its correspondent epipolar line and the profile in the second image.

Figure 8 shows the relative position of the reconstructed object. Incidentally, the camera is far away, making both the motion estimation and the reconstruction an even more challenging problem, since the most appropriate model to deal with such situations is the affine model, instead of the projective model used throughout this paper. Details of the 3D reconstruction of the object are shown in Figure 12 and Figure 13.

## 6 Summary and Conclusions

This paper introduces a novel technique for motion estimation from image profiles. It does not make use of expensive search procedures, such as bundle adjustment, although it naturally integrates data from multiple images. The method is mathematically sound, practical and highly accurate. From the motion estimation to the model reconstruction, no point tracking is required and it does not depend on having point correspondences beforehand.

The convergence to local minima, a critical issue in most non-linear optimisation problems, is avoided by a divide-and-conquer approach which keeps the size of the problem manageable. Moreover, a search space with lower dimension results in fewer iterations before convergence. The quality of model reconstructed is remarkable, in particular if one considers that only the least possible amount of information has been used.

## References

1. K. Åström, R. Cipolla, and P. J. Giblin. Generalised epipolar constraints. In B. F. Buxton and R. Cipolla, editors, *Proc. 4th European Conf. on Computer Vision*, volume II, pages 97–108. Springer-Verlag, 1996.

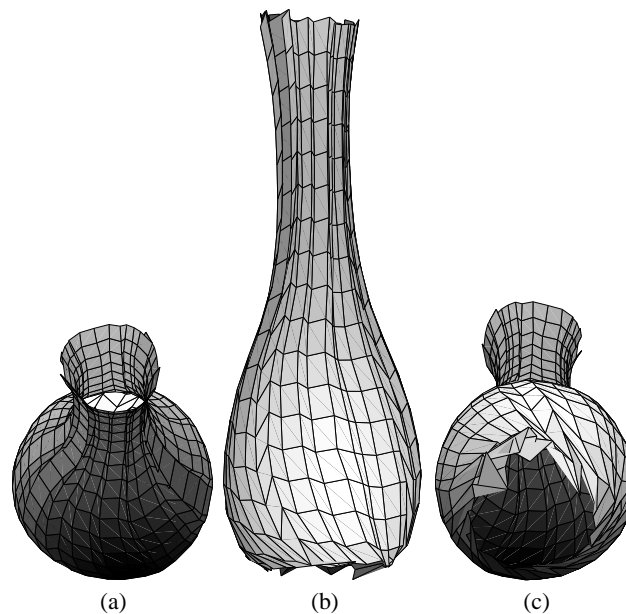


**Fig. 12.** Details of the reconstruction of the object in Figure 3(a). The reconstructed model is smooth, even considering that the epipolar parameterisation is degenerate in the neighbourhood of the frontier points. The views in (a) correspond to an angle  $\psi$  of  $10^\circ$  with respect to the  $y$ -axis. (b)  $\psi = 0^\circ$ . (c)  $\psi = 170^\circ$ . The original viewing direction, computed from the estimated motion, is  $\psi = 24.35^\circ$ .

2. K. Åström and F. Kahl. Motion estimation in image sequences using the deformation of apparent contours. *IEEE Trans. Pattern Analysis and Machine Intell.*, 21(2):114–127, February 1999.
3. H. G. Barrow and J. M. Tenenbaum. Interpreting line drawings as three-dimensional surfaces. *Artificial Intelligence*, 17:75–116, 1981.
4. E. Boyer and M. O. Berger. 3D surface reconstruction using occluding contours. *Int. Journal of Computer Vision*, 22(3):219–233, 1997.
5. R. Cipolla, K. Åström, and P. J. Giblin. Motion from the frontier of curved surfaces. In *Proc. 5th Int. Conf. on Computer Vision*, pages 269–275, 1995.
6. R. Cipolla and A. Blake. Surface shape from the deformation of apparent contours. *Int. Journal of Computer Vision*, 9(2):83–112, 1992.
7. G. Cross, A. Fitzgibbon, and A. Zisserman. Parallax geometry of smooth surfaces in multiple views. In *Proc. 7th Int. Conf. on Computer Vision*, volume I, pages 323–329, 1999.
8. A. W. Fitzgibbon, G. Cross, and A. Zisserman. Automatic 3D model construction for turntable sequences. In *3D Structure from Multiple Images of Large-Scale Environments, European Workshop SMILE'98*, Lecture Notes in Computer Science 1506, pages 155–170, 1998.
9. P. J. Giblin and R. Weiss. Reconstruction of surfaces from profiles. In *Proc. 1st Int. Conf. on Computer Vision*, pages 136–144, London, 1987.
10. P. J. Giblin and R. S. Weiss. Epipolar fields on surfaces. In J-O. Eklundh, editor, *Proc. 3rd European Conf. on Computer Vision*, volume I, pages 14–23. Springer-Verlag, 1994.
11. R. I. Hartley and P. Sturm. Triangulation. *Computer Vision and Image Understanding*, 68(2):146–157, November 1997.
12. R. Koch, M. Pollefeys, and L. Van Gool. Multi viewpoint stereo from uncalibrated video sequences. In *Proc. 5th European Conf. on Computer Vision*, volume I, pages 55–71, 1998.
13. J. J. Koenderink. What does the occluding contour tell us about solid shape? *Perception*, 13:321–330, 1984.
14. P. R. S. Mendonça and R. Cipolla. Estimation of epipolar geometry from apparent contours: Affine and circular motion cases. In *Proc. Conf. Computer Vision and Pattern Recognition*, volume I, pages 9–14, 1999.



**Fig. 13.** Reconstruction of the object in Figure 3(a), showing the shaded surface. The view points are the same as in Figure 12.

15. P. R. S. Mendonça, K-Y. K. Wong, and R. Cipolla. Circular motion recovery from image profiles. In B. Triggs, R. Szeliski, and A. Zisserman, editors, *ICCV Vision and Algorithms Workshop: Theory and Practice*, Corfu, Greece, 21–22 September 1999. Springer-Verlag.
16. J. Porrill and S. B. Pollard. Curve matching and stereo calibration. *Image and Vision Computing*, 9(1):45–50, 1991.
17. J. H. Rieger. Three dimensional motion from fixed points of a deforming profile curve. *Optics Letters*, 11:123–125, 1986.
18. J. Sato and R. Cipolla. Affine reconstruction of curved surfaces from uncalibrated views of apparent contours. In *Proc. 6th Int. Conf. on Computer Vision*, pages 715–720, 1998.
19. J. G. Semple and G. T. Kneebone. *Algebraic Projective Geometry*. Oxford University Press, 1952.
20. R. Vaillant and O. D. Faugeras. Using extremal boundaries for 3D object modelling. *IEEE Trans. Pattern Analysis and Machine Intell.*, 14(2):157–173, 1992.
21. T. Vieville and D. Lingrand. Using specific displacements to analyze motion without calibration. *Int. Journal of Computer Vision*, 31(1):5–29, February 1999.
22. K-Y. K. Wong, P. R. S. Mendonça, and R. Cipolla. Reconstruction and motion estimation from apparent contours under circular motion. In *Proc. British Machine Vision Conference*, pages 83–92, Nottingham, UK, 1999.